Wetting states of two-dimensional drops under gravity

Cunjing Lv[1,2,*] and Songlin Shi[2]

[1]*Institute of Biomechanics and Medical Engineering, AML, Department of Engineering Mechanics, Tsinghua University, Beijing 100084, China*

[2]*CNMM, Department of Engineering Mechanics, Tsinghua University, Beijing 100084, China*

(Received 20 June 2018; published 25 October 2018)

In this study we give an analytical model for the Young-Laplace equation of two-dimensional (2D) drops under gravity. Inspired by the pioneering work of Landau and Lifshitz [*Fluid Mechanics*, 2nd ed. (Pergamon Press, Oxford, 1987), pp. 242–243], we derive general analytical expressions of the profile of drops on flat surfaces, which is available for arbitrary contact angles and drop volumes. We then extend the theoretical model to drops on inclined surfaces and reveal that the contact line plays an important role in determining the wetting state of the drops: (1) when the contact line is completely pinning, the rear and front contact angles and the shape of the drop can be uniquely determined by the drop volume, the slope of the inclined surface, and the contact area; (2) when the contact angle hysteresis is taken into consideration, various mathematical solutions of the wetting state exist for a drop of given volume on a given surface, but there is only one wetting state corresponding to a minimum free energy which results from the competition between the capillary force and gravity. Our theory is in excellent agreement with numerical and experimental results.

DOI: 10.1103/PhysRevE.98.042802

I. INTRODUCTION

When a drop is deposited on a surface, it adopts a specific shape which is governed by the Young-Laplace equation [1,2]. Obtaining the solution of the Young-Laplace equation is fundamentally important for understanding the underlying physics of wetting, such as the capillary force, adhesion and friction at the solid-liquid interface, morphology of the liquid, stability and transition of the wetting state, etc. In the absence of gravity, drops would adopt a spherical shape. Influences such as the gravity and the roughness of the surface are of practical importance in wetting [3–5] and need to be taken into consideration. One of the earliest and most comprehensive efforts addressing the gravitational effect on the shape of a three-dimensional (3D) sessile drop came from Bashforth and Adams [6,7]; however, there is no known closed solution of the Bashforth-Adams equation, so some iterative numerical methods have to be employed. When gravity is considered, the exact (nontrivial) solutions of the Young-Laplace equation have been found only in the cases of (1) a fluid in a semi-infinite domain bounded by a vertical plane wall or (2) for a fluid between two vertical parallel walls. These results were both given by Landau *et al.* [8], and they are solutions for wetting in two-dimensional (2D) space. Moreover, the characteristic size of the study is on the order of the capillary length $a = (\sigma/\rho g)^{1/2}$ [9], in which σ, ρ, and g are the liquid-vapor surface tension, mass density of the liquid, and gravitational acceleration.

Sparked by these seminal works, researchers have resorted to approximate solutions to quantify the relevant questions, such as the shape and contact angle measurement of drops on flat surfaces [7,10–20], pendant drops [21–23], the balance between the surface tension and gravity for drops lying on inclined surfaces [10,24–29], drop-on-fiber systems [9,30], the capillary rise in a wedge or tube [31–35], etc., including both 2D and 3D cases. However, their utility has a limited scope because usually the effect of gravity (which is characterized by the Bond number) was assumed to be very small ($\mathrm{Bo} = \rho g l^2/\sigma \ll 1$, denoting l the size of the drop), or the value of the contact angle θ (which is used to characterize the wettability of the surface) was assumed in some specific regime. When a drop is lying on an inclined surface in the presence of roughness, the question is more complicated. The only known exact relationship is for a 2D case [10],

$$\rho g V \sin\alpha = \sigma(\cos\theta_{\mathrm{rear}} - \cos\theta_{\mathrm{front}}), \tag{1}$$

in which ρ is the areal density of the drop with a cross section V, θ_{rear} and θ_{front} are the rear and front contact angles, and α is the slope of the surface; when it reaches a critical value (i.e., sliding angle) the drop begins to slide down the surface. Equation (1) is simply based on a force balance of different components of the surface tensions and gravity along the inclined surface. In Sec. III we will verify that Eq. (1) is essentially a boundary condition of the Young-Laplace equation for drops lying on inclined surfaces. For the 3D case, Eq. (1) is modified to $\rho g V \sin\alpha = k w \sigma(\cos\theta_{\mathrm{rear}} - \cos\theta_{\mathrm{front}})$, in which w is the width of the solid-liquid contact area and k is a numerical constant that depends on the shape of the drop [26]. Unfortunately, even for given values of α and V, we cannot distinguish θ_{rear} and θ_{front} from Eq. (1) alone. Moreover, we cannot predict the sliding angle via Eq. (1) with certain values of V and the contact angle θ. Considering these open questions, exact (nontrivial) solutions of the Young-Laplace equation for drops under gravity have remained to be explored further, and more modeling efforts are still needed.

*cunjinglv@tsinghua.edu.cn

In the present study, we restrict our analysis to the 2D problem of drops having a size on the order of the capillary length, which is a natural extension of the seminal works on 2D wetting [8,10,25], and this simplification is easier to tackle than the 3D problem. In fact, 2D results have considerable practical applications to industrial problems, such as the dip-coating and printing processes, deposition and solidification of molten materials, anisotropic wettability on striped surfaces for fluidic control, and directional transport of liquid on solids [36–40]. In these cases, the dimension of the liquid in one direction is much larger than it is in the other direction, so the cross section could be approximately assumed to be a 2D case. Recently, interest in 2D geometry has increased, and some results suggest that the physics are almost indistinguishable between the 2D and 3D cases such as in liquid spreading, wettability of drops on soft solids, and motion of long bubbles in channels [41–44]. Here we derive exact analytical solutions of the Young-Laplace equation for 2D drops lying on both flat and inclined surfaces. We not only exactly determine all related quantities (V, the rear and front contact angles, the profile of the liquid, contact region, free energy, etc.) without any assumption or approximation, but also reveal the dependencies among them.

II. GENERAL SOLUTION OF THE SHAPE OF DROPS LYING ON A HORIZONTAL SURFACE

As shown in Fig. 1, we demonstrate the exact profiles of two drops lying on horizontal surfaces under gravity in 2D space. Practically, these shapes correspond to cross sections of a liquid on surfaces of the aforementioned cases [36–40]. The shape of the drop is governed by the Young-Laplace equation $\kappa\sigma = \Delta p$, where κ and Δp are the curvature and pressure difference between the liquid and vapour phases at any point of the meniscus. In Fig. 1 the Young-Laplace equation can be expressed as

$$\frac{z''}{[1+(z')^2]^{3/2}}\,\sigma = \Delta p_0 + \rho g z, \tag{2}$$

in which Δp_0 is a constant. Previously researchers employed various approximate methods to solve Eq. (2). The term z' was usually ignored (i.e., let $\kappa \approx z''$), and this view obtained a great success in the field of lubrication [4], but the solution is limited to small contact angles. For high contact angles, researchers employed perturbation methods and approximate solutions [7,16–20] and could also get good results, even though there is still a lack of comprehensive understanding, and a general solution which can be applied to any value of the contact angle remains unaddressed.

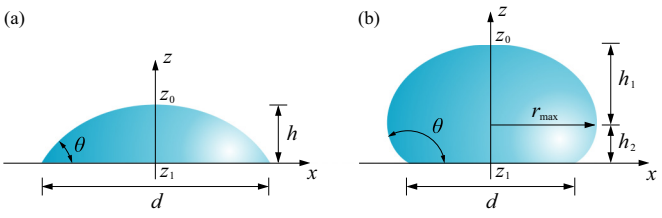

FIG. 1. Wetting states of 2D drops on horizontal surfaces under gravity. These profiles are obtained using Eqs. (4) and (5): (a) $\theta = 60^\circ$, $d = 2a$; (b) $\theta = 150^\circ$, $d = 2a$ (the origin of the coordinate system is not at the center of the solid-liquid contact area; see Fig. 8).

The exact solutions of the Young-Laplace equation under gravity obtained by Landau *et al.* [8] are applicable only to the profile of menisci bounded by one or two vertical planes. However, the modeling could be extended to derive exact analytical solutions of the wetting state of sessile drops under gravity. To our best knowledge, the exact solution of Eq. (2) for 2D drops under gravity has not been reported previously (see Appendixes A 1 and A 2). We obtain

$$V = 2a^2\left[\sqrt{A-\cos\theta}\int_0^\theta \frac{\cos\xi}{\sqrt{A-\cos\xi}}\,d\xi - \sin\theta\right], \tag{3}$$

$$x = \pm\frac{\sqrt{2}a}{2}\int_0^\eta \frac{\cos\xi}{\sqrt{A-\cos\xi}}\,d\xi, \quad \eta\in[0,\theta], \tag{4}$$

$$z = -\sqrt{2}a\sqrt{A-\cos\eta}, \quad \eta\in[0,\theta]. \tag{5}$$

For a drop of given volume on a given surface (in other words, θ and V are known parameters), A is a constant ($A \in [1,\infty]$) which is uniquely defined by Eq. (3). Subsequently, the profile of the liquid-vapor meniscus can be obtained using Eqs. (4) and (5). (Note: in Fig. 1 the origin of the coordinate system is not at the center of the solid-liquid contact area; see Fig. 8.) According to Eqs. (4) and (5), we further obtain the width d of the solid-liquid contact area and the height h of the drop:

$$d = \sqrt{2}a\int_0^\theta \frac{\cos\xi}{\sqrt{A-\cos\xi}}\,d\xi, \tag{6}$$

$$h = \sqrt{2}a(\sqrt{A-\cos\theta}-\sqrt{A-1}). \tag{7}$$

Moreover, we use w and $r_{\max}$ to denote the width and half-width of the liquid phase, $w = 2r_{\max}$. When $0^\circ \leqslant \theta \leqslant 90^\circ$, we have $w = d = 2r_{\max}$; when $90^\circ < \theta \leqslant 180^\circ$, we have $w = 2r_{\max} > d$ with

$$r_{\max} = \frac{\sqrt{2}a}{2}\int_0^{\pi/2} \frac{\cos\xi}{\sqrt{A-\cos\xi}}\,d\xi, \tag{8}$$

$$h_1 = \sqrt{2}a(\sqrt{A}-\sqrt{A-1}),$$
$$h_2 = \sqrt{2}a(\sqrt{A-\cos\theta}-\sqrt{A}), \tag{9}$$

where $h_1 = z_0 - z|_{r=r_{\max}}$, $h_2 = z|_{r=r_{\max}} - z_1$, and $h = h_1 + h_2$. A combination of Eqs. (3) and (6) leads to

$$V = 2a^2\left[\frac{\sqrt{2}}{2}\left(\frac{d}{a}\right)\sqrt{A-\cos\theta} - \sin\theta\right]. \tag{10}$$

There are two cases which are valuable to be discussed. First, when $A \to \infty$, we get $d \approx \sqrt{2}a\sin\theta/\sqrt{A}$ and $h \approx \sqrt{2}a(1-\cos\theta)/2\sqrt{A}$ from Eqs. (6) and (7), respectively, which results in $h/d \approx (1-\cos\theta)/2\sin\theta$. This case corresponds to very small droplets with a spherical shape because the effect of gravity can be ignored. Second, when $A \to 1$,

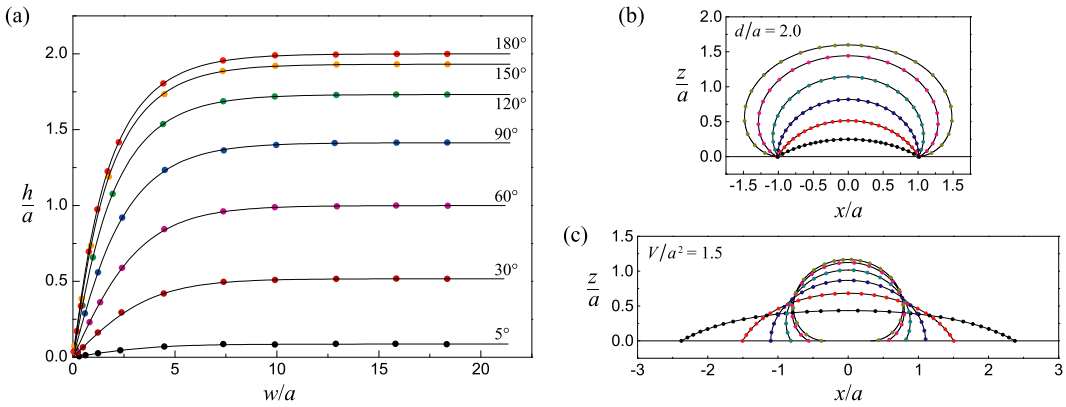

FIG. 2. Comparisons between theoretical [solid curves, the solutions of Eqs. (6)–(8)] and numerical results [dots, the solutions of Eq. (2)]: (a) The dependency of h/a on w/a. The contact angle θ ranges from 5° to 180°. When w/a is large enough, $h/a \to 2\sin(\theta/2)$ [9], as the plateau shown in each curve. (b), (c) Profiles of drops with a fixed solid-liquid contact region $d/a = 2.0$ and a fixed volume $V/a^2 = 1.5$, respectively. Different curves (bottom-up) correspond to $\theta = 30°, 60°, 90°, 120°, 150°, 180°$. The x axis and z axis shown in (b) and (c) are in scale.

we get $d \to \infty$ and $h \approx 2a\sin(\theta/2)$ [9], which indicates big puddles. In the latter case, when $\theta \in [90°, 180°]$, Eq. (9) reduces to $h_1 \approx \sqrt{2}a$, $h_2 \approx \sqrt{2}a[\sqrt{2}\sin(\theta/2) - 1]$. This suggests h_1 is approximately constant and h relies just on h_2. This essentially implies that if we focus just on the upper part of the liquid [$z \geqslant z|_{r=r_{\max}}$ in Fig. 1(b)], we always get a nominal puddle with $\theta = 90°$. Moreover, when $A \to 1$ ($d \to \infty$), the profile of the liquid-vapor interface of a half puddle (e.g., the part when $x \leqslant 0$) is similar to the meniscus of an infinitely long cylinder pressing at a liquid-air interface, which has received a lot of interest in recent years [45,46].

In order to check the validity of the above theoretical results, we carry out numerical calculations by employing a finite element method (Surface Evolver [47]) and make comparisons between these two ways. In Fig. 2(a) we give the dependency of h on w. Moreover, we also focus on specific cases: we fix the dimensionless values of the solid-liquid contact area at $d/a = 2.0$ and the volume at $V/a^2 = 1.5$ in Figs. 2(b) and 2(c), respectively, but vary the contact angle ($\theta \in [30°, 180°]$). The solid curves represent results obtained using Eqs. (3)–(5), and the dots are numerical results extracted from Surface Evolver. Moreover, we also carry out experiments systematically by employing a commercial contact angle measurement (OCA20, Dataphysics, Germany). Considering producing a 2D drop is challenging, but by employing patterns with hydrophilic and superhydrophobic regions (details are given in Appendix B), we produce liquid strips, and its appearance observed from the side view could be approximately treated as the profile of a 2D droplet. First, as shown in Fig. 3, we give the evolution of the liquid profiles with the apparent contact angle (or the area of the cross section) on horizontal substrates (the left column). In these cases, the width of the contact region is fixed at $d = 6.3$ mm, and the apparent contact angles range from $\theta = 36.3°$ to $\theta = 118.7°$. To make comparisons, we superpose the theoretical results (using hollow red circles) on the experimental frames, which repeats the experiments very well. The comparisons demonstrated in Figs. 3 and 4 suggest that the theory, numerical, and experimental results are in an excellent agreement with each other.

III. DROPS LYING ON AN INCLINED SURFACE

By employing the same approach but with modified boundary conditions (Appendix A 3), we can quantify the wetting state of drops on inclined surfaces. As shown in Fig. 4, we define d as the width of the solid-liquid area and H as the altitude difference between the left and right contact lines.

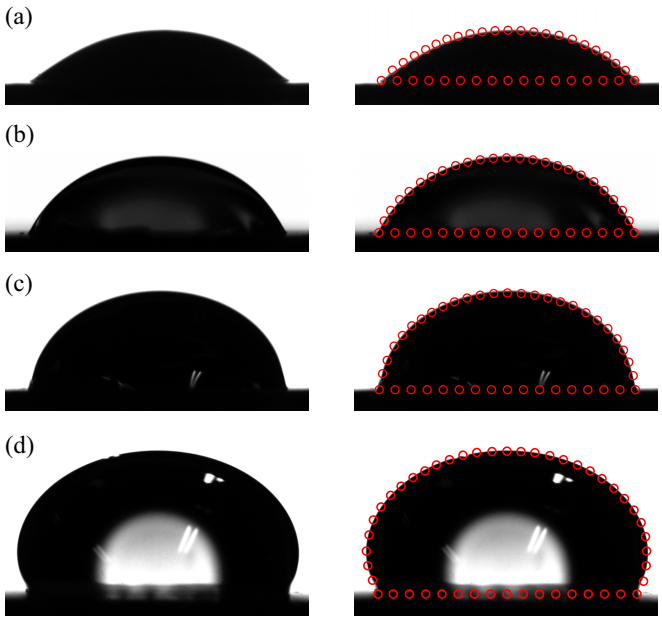

FIG. 3. Comparison of the experimentally and theoretically obtained liquid profiles. The theoretical results are obtained using Eqs. (3)–(5) and are represented as hollow red circles. For each wetting state, the left one is the original experimental image, and the right one shows the comparison. The width of the solid-liquid contact region is $d = 6.3$ mm. The corresponding contact angles and areas of the cross section are (a) $\theta = 36.3°$, $A = 5.5$ mm^2; (b) $\theta = 67.5°$, $A = 8.5$ mm^2; (c) $\theta = 87.5°$, $A = 11.5$ mm^2; (d) $\theta = 118.7°$, $A = 19.5$ mm^2. The scale bar represents 2.0 mm.

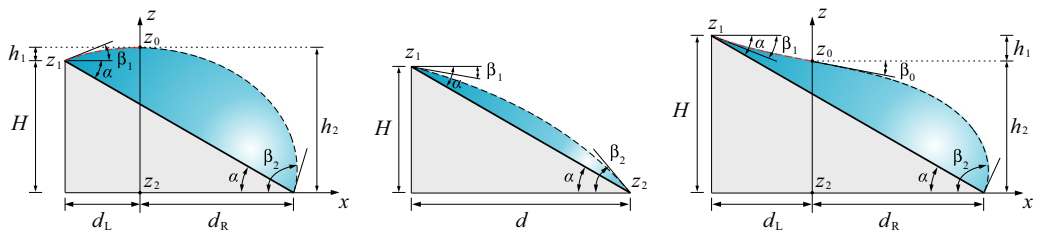

FIG. 4. Definitions of the geometrical parameters for drops lying on inclined surfaces. α is the slope of the surface, $d = d_L + d_R$ is the projected length of the solid-liquid contact area d_{SL} on the x axis, and $H = z_1 - z_2$ is the altitude difference between the rear and front contact lines. We define $\theta_{rear} = \beta_1 + \alpha$ and $\theta_{front} = \beta_2 - \alpha$, respectively: (a) $\theta_{rear} \geqslant \alpha$, (b) $\theta_{rear} \leqslant \alpha$, and (c) $\theta_{rear} \leqslant \alpha$ and the liquid-vapor meniscus consists of a concave and a convex part (more details are given in Fig. 9).

For convenience, we define $\theta_{rear} = \beta_1 + \alpha$ and $\theta_{front} = \beta_2 - \alpha$ as the apparent contact angles at the rear and the front contact points. We have the following three cases. In the first two cases, $\theta_{rear} \geqslant \alpha$ and $\theta_{front} \leqslant \alpha$ (which means $\beta_1 \leqslant 0$) as shown in Figs. 4(a) and 4(b), respectively, the profiles of the liquid-vapor interface are globally convex and for convenience can be characterized using the following unified formulas:

$$H = \sqrt{2}a(\sqrt{A - \cos\beta_2} - \sqrt{A - \cos\beta_1}), \tag{11}$$

$$d = \frac{\sqrt{2}a}{2}\left(\int_0^{\beta_1} \frac{\cos\xi}{\sqrt{A - \cos\xi}}\,d\xi + \int_0^{\beta_2} \frac{\cos\xi}{\sqrt{A - \cos\xi}}\,d\xi\right). \tag{12}$$

In fact, we can write d as $d = d_L + d_R$ with

$$d_L = \frac{\sqrt{2}a}{2}\int_0^{\beta_1} \frac{\cos\xi}{\sqrt{A - \cos\xi}}\,d\xi,$$
$$d_R = \frac{\sqrt{2}a}{2}\int_0^{\beta_2} \frac{\cos\xi}{\sqrt{A - \cos\xi}}\,d\xi, \tag{13}$$

and H as $H = h_2 - h_1$ with

$$h_1 = \sqrt{2}a(\sqrt{A - \cos\beta_1} - \sqrt{A - 1}),$$
$$h_2 = \sqrt{2}a(\sqrt{A - \cos\beta_2} - \sqrt{A - 1}). \tag{14}$$

For the case in Fig. 4(b), d_L, d_R, h_1 and h_2 are virtual geometrical parameters and not shown. In these first two cases, A is still a coefficient and $A \in [1, \infty]$.

However, if the solid-liquid contact area d_{SL} is large enough, as shown in Fig. 4(c), $\theta_{rear} \leqslant \alpha$ (which also means $\beta_1 \leqslant 0$), the liquid-vapor meniscus consists of a concave (on the left) and a convex (on the right) parts. In this case, we obtain

$$H = \sqrt{2}a(\sqrt{A - \cos\beta_1} + \sqrt{A - \cos\beta_2}), \tag{15}$$

$$d = \frac{\sqrt{2}a}{2}\left(\int_{\beta_0}^{-\beta_1} \frac{\cos\xi}{\sqrt{A - \cos\xi}}\,d\xi + \int_{\beta_0}^{\beta_2} \frac{\cos\xi}{\sqrt{A - \cos\xi}}\,d\xi\right), \tag{16}$$

in which $\beta_0 (\geqslant 0)$ means the slope of the meniscus at z_0 (the curvature $\kappa|_{z_0} = 0$), and in this case $A = \cos\beta_0 \in [0, 1]$. We can write d as $d = d_L + d_R$ with

$$d_L = \frac{\sqrt{2}a}{2}\int_{\beta_0}^{-\beta_1} \frac{\cos\xi}{\sqrt{A - \cos\xi}}\,d\xi,$$
$$d_R = \frac{\sqrt{2}a}{2}\int_{\beta_0}^{\beta_2} \frac{\cos\xi}{\sqrt{A - \cos\xi}}\,d\xi, \tag{17}$$

and $H = h_1 + h_2$ with

$$h_1 = \sqrt{2}a(\sqrt{A - \cos\beta_1}),$$
$$h_2 = \sqrt{2}a(\sqrt{A - \cos\beta_2}). \tag{18}$$

Similarly to calculating the morphology of the drop on the horizontal surface, i.e., using Eqs. (4)–(7), the profile of the drop on the inclined surface can also be obtained. When we take the value of ξ between $[\beta_0, \beta_1]$ and $[\beta_0, \beta_2]$ in Eqs. (13) and (14) [or Eqs. (17) and (18)], we can get the corresponding values of (x, z) and the whole profile of the drop, as shown in Figs. 5(a) and 5(c).

Interestingly, one can imagine that if d is larger than a critical value, there will be no existence of physical solution of the above equations for a sessile drop. Instability and wetting transition would happen, and the liquid would break up. In this case, dynamics would be involved, and the corresponding behaviors are complicated and beyond the scope of this paper. For further discussion, see the recent Refs. [48–50].

Moreover, the volume of the drops in Fig. 4 can be obtained (see Appendix A 3):

$$\frac{V}{a^2} = \frac{1}{\tan\alpha}[\cos\beta_1 - \cos\beta_2] - [\sin\beta_1 - \sin\beta_2]. \tag{19}$$

Multiplying $\rho g a^2 \sin\alpha$ on both sides of Eq. (19) leads to Eq. (1), which means that Eq. (1) is indeed a natural boundary condition of the Young-Laplace equation.

In the following, two situations will be discussed: (1) a completely pinning of the contact line and (2) when the contact angle hysteresis and a movability of the contact line are taken into consideration.

A. Complete pinning of the contact line

As a consequence of the inevitable roughness of real surfaces, the contact line pinning is a very common

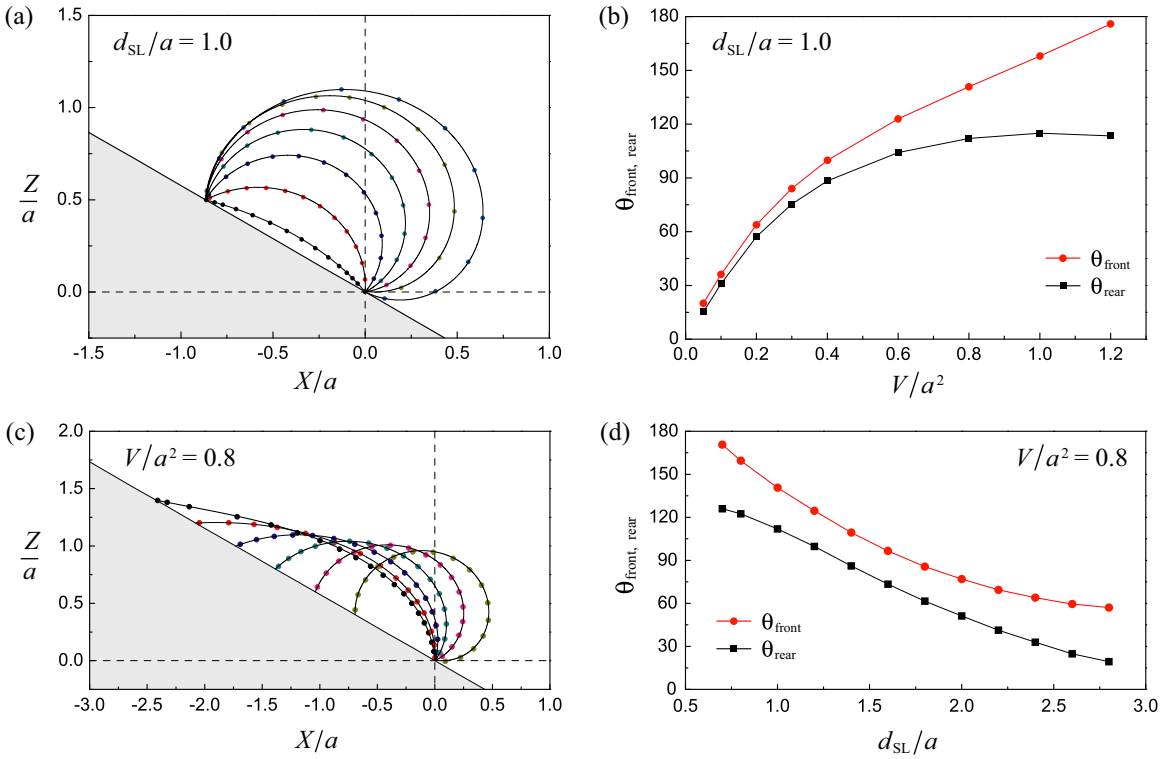

FIG. 5. Profile of drops on inclined surfaces with $\alpha = 30^\circ$: (a) $d_{SL}/a = 1.0$, the volume varies as $V/a^2 = 0.05, 0.2, 0.4, 0.6, 0.8, 1.0, 1.2$; (c) $V/a^2 = 0.8$, the solid-liquid area varies as $d_{SL}/a = 0.8, 1.2, 1.6, 2.0, 2.4, 2.8$. The solid curves are theoretical results and the dots are numerical results extracted from Surface Evolver. In (b) and (d), the variation of θ_{rear} and θ_{front} are given, corresponding to (a) and (c), respectively. The red dots and black squares are theoretical results with the solid curves as a guide to the eye.

phenomenon [9]. If the contact line is completely pinned, for a specific case (i.e., a drop of given volume on a given inclined surface with a given solid-liquid contact area), V, α, and d_{SL} are given, so $d = d_{SL}\cos\alpha$ and $H = d_{SL}\sin\alpha$ are also known. Combining Eqs. (1), (11), and (12) [or Eqs. (15) and (16)] (recall we have defined $\beta_1 = \theta_{rear} - \alpha$ and $\beta_2 = \theta_{front} + \alpha$), the three unknown parameters (A, θ_{rear}, and θ_{front}) can be found by solving these three equations. This case is very different from the case in Sec. II, in which the only one unknown parameter A is solely determined by using Eq. (3). Two examples of drops lying on an inclined surface with $\alpha = 30^\circ$ are demonstrated in the following. First, in Fig. 5(a), the solid-liquid contact area is fixed at $d_{SL}/a = 1.0$. Different curves correspond to drops with different volumes, $V/a^2 \in [0.05, 1.2]$. Second, in Fig. 5(c) the volume of the drop is fixed at $V/a^2 = 0.8$ with a variation of the solid-liquid contact area $d_{SL}/a \in [0.8, 2.8]$. The solid curves are theoretical results, which agree well with numerical results (dots) extracted from Surface Evolver. We give the variation of θ_{rear} and θ_{front} in Figs. 5(b) and 5(d), corresponding to Figs. 5(a) and 5(c), respectively. Moreover, based on the same setup as shown in Fig. 3 and Appendix B, we tilt the substrate to obtain the wetting state of 2D drops, and their side views are shown in Fig. 6. In this cases, the width of the contact region is also fixed at $d = 6.3$ mm. The areas of the cross section of the frames are similar to each other but with a distinguished slope of the substrate ranging from $\alpha = 8.0^\circ$ to 60.0°, so the rear contact angles θ_{rear} and front contact angles θ_{front} are very different from each other in different frames. To make comparisons, we superpose the theoretical results (hollow red circles) on the experimental frames, which shows our theory repeats the experiments very well.

The achievement of the above exact solutions of the Young-Laplace equation guarantees a direct evaluation of a broad range of physical quantities, which plays an important role for further understanding of the underlying mechanism in wetting. For example, one can calculate the free energy of the drop, which includes two parts, the surface energy E_s and gravitational potential E_g, so $E = E_s + E_g$. E_s is defined using

$$\begin{aligned} E_s &= \sigma S_{LV} + (\sigma_{SL} - \sigma_{SV}) d_{SL} \\ &= \sigma (S_{LV} - d_{SL}\cos\theta_Y) \end{aligned} \tag{20}$$

in which θ_Y is the Young contact angle and defined using $\cos\theta_Y = (\sigma_{SV} - \sigma_{SL})/\sigma$ [1], denoting σ, σ_{SV}, and σ_{SL} the liquid-vapor, solid-vapor, and solid-liquid interfacial tensions, respectively. S_{LV} is the arc length of the liquid-vapor interface. Considering E_g depends on relative position, we need a reference level ($Z = 0$) at which to set the potential energy equal to 0. For convenience, we always set the front point of the solid-liquid area at $X = 0$ and $Z = 0$, as shown in Figs. 5(a) and 5(c). The reference level will not alter the physics in this problem.

Finally, we obtain the normalized total free energy for Figs. 4(a) and 4(b):

$$\frac{E}{a\sigma} = \frac{\sqrt{2}}{2}\left(\int_0^{\beta_1} \frac{A\cos\xi + \sin^2\xi}{\sqrt{A-\cos\xi}}\,d\xi + \int_0^{\beta_2} \frac{A\cos\xi + \sin^2\xi}{\sqrt{A-\cos\xi}}\,d\xi\right) + \frac{\sqrt{2}V}{a^2}\sqrt{A-\cos\beta_2} - \frac{1}{6}\left(\frac{d}{a}\right)^3 \tan^2\alpha - \left(\frac{d}{a}\right)\left[\sqrt{(A-\cos\beta_1)(A-\cos\beta_2)} + \frac{\cos\theta_Y}{\cos\alpha}\right]. \tag{21}$$

For Fig. 4(c), we obtain

$$\frac{E}{a\sigma} = \frac{\sqrt{2}}{2}\left(\int_{\beta_0}^{-\beta_1} \frac{A\cos\xi + \sin^2\xi}{\sqrt{A-\cos\xi}}\,d\xi + \int_{\beta_0}^{\beta_2} \frac{A\cos\xi + \sin^2\xi}{\sqrt{A-\cos\xi}}\,d\xi\right) + \frac{\sqrt{2}V}{a^2}\sqrt{A-\cos\beta_2} - \frac{1}{6}\left(\frac{d}{a}\right)^3 \tan^2\alpha + \left(\frac{d}{a}\right)\left[\sqrt{(A-\cos\beta_1)(A-\cos\beta_2)} - \frac{\cos\theta_Y}{\cos\alpha}\right]. \tag{22}$$

From the definition of E_s in Eq. (20), we know that for a complete contact line pinning case, $d_{SL}\cos\theta_Y$ is a constant, so the Young contact angle θ_Y has no contribution for determining the profile of the liquid-vapor meniscus. In other words, let us give insight in view of energy. For given values of V, α, and d_{SL}, there are infinite mathematical solutions of the liquid profile (correspond to various values of A, θ_{rear}, and θ_{front}), but the one in the real case must be with the minimum free energy (i.e., corresponding to $\delta E = 0$), and the solutions are Eqs. (1), (11), and (12) [or (15) and (16)]. Since $\delta(d_{SL}\cos\theta_Y) = 0$, so the intrinsic contact angle θ_Y contributes only to the value of the total free energy.

Moreover, the results obtained in this section are consistent with the results of the drop lying on a flat surface ($\alpha = 0^\circ$). In Sec. I we never introduce any contact angle hysteresis or line pinning, so $\theta = \theta_{rear} = \theta_{front}$, and Eqs. (12) and (14) degrades to Eqs. (6) and (7), respectively. For a drop of given V and θ, A can be determined from Eq. (3), and then d can be determined naturally from Eq. (6) [otherwise, if V and d are known, A and the apparent contact angle θ can also be determined by the combination of Eqs. (6) and (10)].

B. Movable contact line

As shown in Sec. III A, for a drop of given volume V on an inclined surface with a certain value of α, if d_{SL} is fixed, θ_{rear}, θ_{front} and the profile of the liquid phase are fixed. However, in practice contact angle hysteresis is observed, the apparent contact angle could take values ranging from the so-called advancing (maximal) contact angle θ_A to the receding (minimal) contact angle θ_R. In this section we take consideration of the contact angle hysteresis and discuss a situation if the drop could have different values of d_{SL}, θ_{rear}, and θ_{front} ($\theta_R \leqslant \theta_{rear} < \theta_{front} \leqslant \theta_A$).

As one example, we fix the volume of the drop and the slope of the inclined surface at $V/a^2 = 0.8$ and $\alpha = 30^\circ$, respectively. For different values of d_{SL}, θ_{rear} and θ_{front} could take different values, and the shape of the drop could take different profiles as well [see Figs. 5(c) and 5(d)]. However, one can imagine that among these possible wetting states, the total free energy of the drop would be different. If the contact line does not pin seriously, the drop might adjust its shape (e.g., though varying d_{SL}) and choose a wetting state with the minimum free energy.

To verify our conclusion, we give the dependency of E (the red circular dots) on d_{SL} as shown in Fig. 5. We can see there is a minimum value (E_{min}) exists, and this state can be exactly characterized by a combination of [based on Eq. (21) or (22)]

$$\frac{dE}{dd_{SL}} = 0 \tag{23}$$

and Eqs. (1), (11), and (12) [or Eqs. (15) and (16)]. The four unknown parameters [A, θ_{rear}, θ_{front}, and d_{SL} (or d)] can be thereby uniquely determined by these four equations. Therefore, we find the wetting state with E_{min} (maybe the most likely wetting state) when the contact angle hysteresis is involved.

Unfortunately, the problem is further complicated by the fact that A, θ_{rear}, θ_{front}, and d_{SL} are functions of each other and they are coupled. So far we could not express Eq. (23) using an explicit formula, and we leave this open question for further research. Instead, by employing a numerical method, we can solve these four equations and find the corresponding wetting state. We mark the resulting E_{min} and d_{SL} in Fig. 7 using a green asterisk. In Fig. 7, $E_{min}/a\sigma$ corresponds to $d_{SL}/a \approx 1.34$.

Moreover, from Figs. 5(c) and 5(d), we can see the mathematical solution of the apparent contact angle θ_{rear} and θ_{front} exists over quite a large range. However, in the real material system, the apparent contact angle usually falls between a limited scope, $\theta \in [\theta_R, \theta_A]$, which indicates that even though we have constructed a closed solution to determine the wetting state of sessile drops, the mathematical model still could not include all the physics. Figure 7 shows that some of the wetting state owns a relative larger free energy, for instance, $d_{SL}/a = 2.8$ compared with $d_{SL}/a = 1.34$, so maybe it is the reason why such state could not exist in practice. Moreover, even real materials could exhibit similar contact angles, and the contact angle hysteresis could be completely different. For example, a very high contact angle could be achieved on the petal's surface of a rose, but a very high adhesive force exists between the surface and sessile drops [51]. So influences such as adhesion, the ability of the liquid meniscus to detach from the surface, the strength of the contact line pinning, etc., have to be taken into consideration. These influences may result from the properties of specific material and liquid systems and need to be involved by employing more elaborate models in the future.

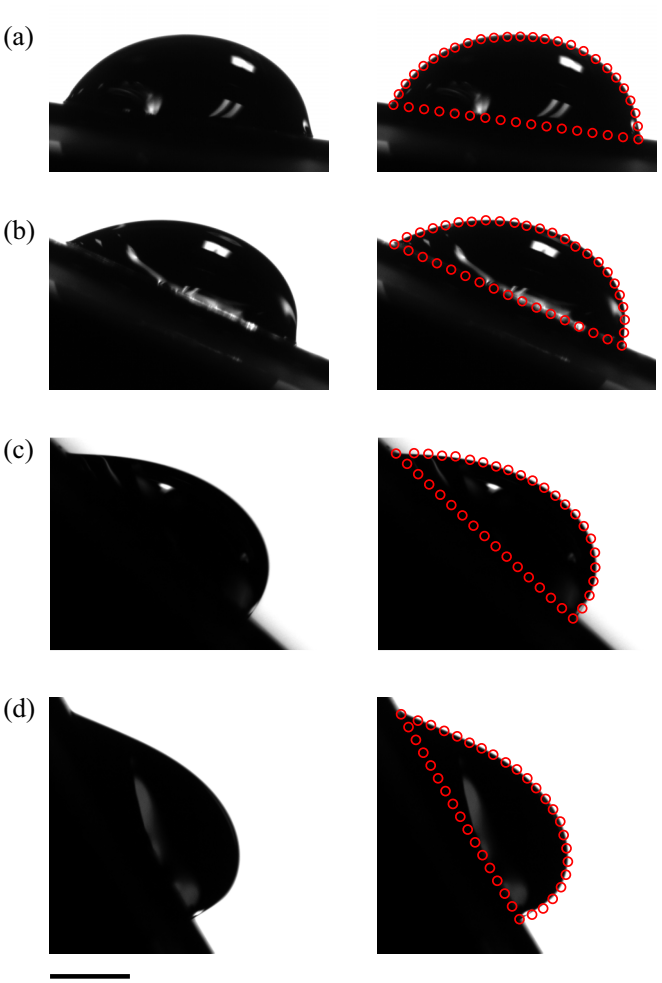

FIG. 6. Comparison of the experimentally and numerically obtained liquid profiles on tilted substrates with $d = 6.3$ mm. Frames on the right column is the combination of original experimental frames (on the left column) and the theoretical results (hollow red circles). The corresponding parameters α, A, θ_{rear}, and θ_{front} are (a) 8.0°, 10.4 mm^2, 67.1°, 72.3°; (b) 24.0°, 8.4 mm^2, 48.1°, 79.0°; (c) 43.0°, 9.0 mm^2, 39.2°, 86.9°; (d) 60.0°, 9.9 mm^2, 33.9°, 98.2°. The scale bar represents 2.0 mm.

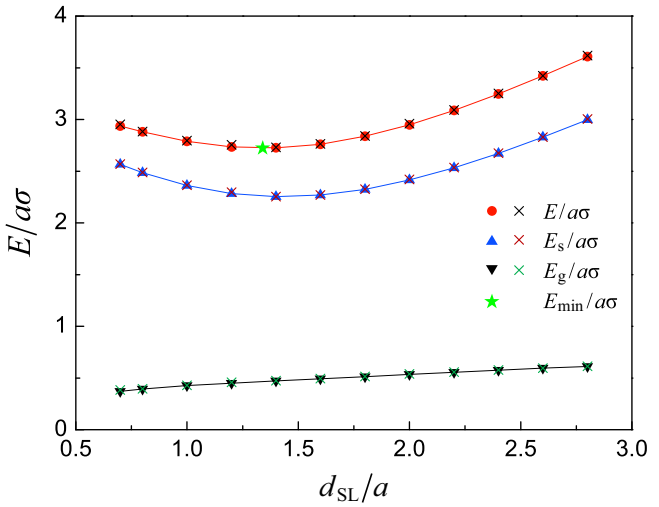

FIG. 7. Dependency of the normalized energy $E/a\sigma$ on d_{SL}/a. These results correspond to Figs. 5(c) and 5(d), in which $V/a^2 = 0.8$ and $\alpha = 30°$. The red circular dots and blue upward-pointing and black downward-pointing triangles represent numerical results (Surface Evolver) of E, E_{s}, and E_{g}, respectively. The cross symbols are the corresponding theoretical results. The green star indicates a wetting state corresponding to $E_{\text{min}}/a\sigma$.

IV. CONCLUDING REMARKS

In this paper we have derived exact analytical solutions of the Young-Laplace equation for 2D drops under gravity, which allow the shape of the drops and other related geometrical parameters (e.g., d, h, θ_{rear}, and θ_{front}) to be fully determined. The excellent agreement between the experimental and theoretical results demonstrated makes such solutions good candidates for the description of 2D drops beyond the capabilities of the lubrication approximation or other types of perturbation solutions (in powers of Bo as the small parameter). Although 2D drops are of theoretical (rather than practical) interest, the existence of an exact analytical solution is a potentially useful step for future studies of industrial processes in a 2D case [36–40].

We believe that the results presented in this work provide a rather important platform for extensions of a number of fundamental directions in wetting. First, instead of constant values of α and V, we could investigate the dependency of θ_{rear}, θ_{front}, and d_{SL} on α or V. We believe there are some critical parameters that account for a series of interesting phenomena, such as when the rear contact line will break up, when the drop will run down the slope, etc. Second, introducing contact angle hysteresis $\Delta\theta$ and assuming $\theta_{\text{rear}} = \theta - \Delta\theta/2$ and $\theta_{\text{front}} = \theta + \Delta\theta/2$ may give us perspectives from a different view. Third, since elliptic integrals are widely utilized, we suggest finding explicit expressions using an asymptotic way built on the exact solutions we have constructed, which would be easier to use and more robust than previous methods which rely on various approximations ($z' \approx 0$ or Bo $\ll 1$). Fourth, considering that interactions are particularly important near the solid-liquid-vapor three-phase contact line, additional contributions such as the Derjagin's disjoining pressure and the elasto-capillarity [9] are worth being explored in further study.

ACKNOWLEDGMENTS

C.L. would like to gratefully acknowledge the support from the Alexander von Humboldt Foundation of Germany, the National Natural Science Foundation of China (Grant No. 11632009), and Tsinghua University (Grant No. 53330100318), Beijing, China. We thank Evan Spruijt and Aditya Bandopadhyay for their help to improve the paper, and the reviewers for their valuable feedback.

APPENDIX A: MODELING AND DEDUCTION OF THE GENERAL SOLUTION

Differently from the work of Landau *et al.* [8], in which they considered only a hydrophilic case and the contact angles between the liquid and each side of the two walls are equal [Fig. 8(a)], we extend the discussion to arbitrary contact angles ($\alpha \in [0°, 180°]$ and $\alpha_1 \neq \alpha_2 \neq \alpha_3 \neq \alpha_4$). Built on these,

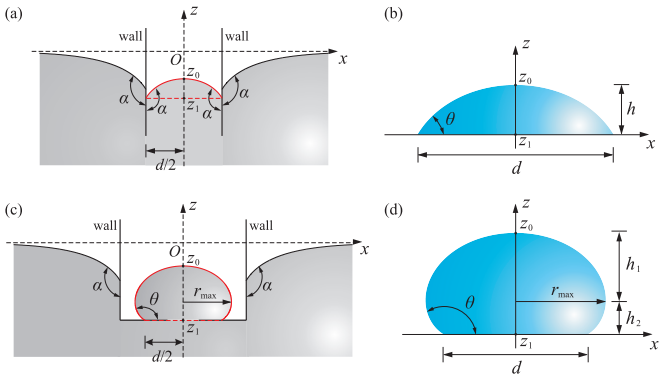

FIG. 8. Wetting and modeling: (a) a 2D meniscus between two plates under gravity. $\alpha = 150^\circ$, $d/2 = a$; (b) a 2D drop under gravity. $\theta = \alpha - \pi/2 = 60^\circ$, $d = 2a$; (c) a 2D meniscus between two plates under gravity. $\alpha = 150^\circ$, and there is a gap between the bottom walls; a drop is formed with $\theta = \alpha = 150^\circ$ and $d/2 = a$; (d) a 2D drop under gravity. $\theta = 150^\circ$, $d = 2a$.

we can find exact solutions of the Young-Laplace equation for 2D drops on horizontal and inclined surfaces.

1. Hydrophilic state

The key idea is that when we make a comparison between Figs. 8(a) and 8(b), we can conclude that the shape enclosed by the meniscus between the two walls and the horizontal dashed line in Fig. 8(a) (as shown in red) is the same as the shape of the 2D drop in Fig. 8(b) in the case (1) $\theta = \alpha - \pi/2$ or (2) the distance between the two walls is equal to the width of the 2D drop. This analysis suggests if we can obtain the profile of the meniscus in Fig. 8(a), we can get the profile of the 2D drop in Fig. 8(b).

On the basis of the Young-Laplace equation [Eq. (2)] and the boundary conditions as shown in Fig. 8(a) $z|_{x\to\infty} = 0$, $z'|_{x\to\infty} = 0$, $z''|_{x\to\infty} = 0$, we get

$$\frac{z}{a^2} - \frac{z''}{[1+(z')^2]^{3/2}} = 0. \tag{A1}$$

A first integral of Eq. (A1) leads to

$$\frac{z^2}{2a^2} = A - \frac{1}{\sqrt{1+(z')^2}}, \tag{A2}$$

in which A is a constant. We have to emphasize that Eqs. (A1) and (A2) are both valid for any part of the meniscus (in other words, the menisci inside and outside of the two vertical parallel walls) even though the menisci are not continuous at the wall. However, the differential equation cannot be solved over the entire domain $x \in [-\infty, \infty]$. To obtain the solution of the profile of the meniscus, corresponding boundary conditions of each part have to be taken into consideration. Here we just focus on the meniscus between the two walls. Regarding $z'|_{x=0} = 0$ and $z'|_{x=d/2} = 1/\tan\alpha$, we can obtain $z_0 = z|_{x=0} = -\sqrt{2}a\sqrt{A-1}$ and $z_1 = z|_{x=d/2} = -\sqrt{2}a\sqrt{A-\sin\alpha}$.

By using a transformation [8] $z = -\sqrt{2}a\sqrt{A-\cos\xi}$, in which ξ is a variable and $\xi \in [0, \alpha - \pi/2]$, and replacing α by $\theta = \alpha - \pi/2$, we can get the values of x, z, and V [see Eqs. (3)–(5)]:

$$x = \int_0^\eta \frac{dx}{dz}\frac{dz}{d\xi}d\xi = \frac{\sqrt{2}a}{2}\int_0^\eta \frac{\cos\xi}{\sqrt{A-\cos\xi}}d\xi, \quad \eta \in [0,\theta], \tag{A3}$$

$$V = 2\int_0^{d/2} z\,dx = 2\int_0^\theta z\frac{dx}{dz}\frac{dz}{d\xi}\,d\xi = 2a^2\left[\sqrt{A-\cos\theta}\int_0^\theta \frac{\cos\xi}{\sqrt{A-\cos\xi}}\,d\xi - \sin\theta\right]. \tag{A4}$$

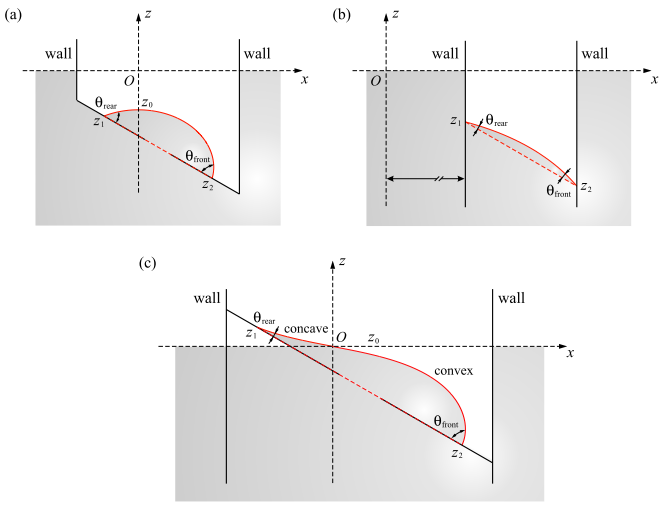

FIG. 9. Modeling and calculations of the menisci. The black solid lines represent solid walls in a liquid. There are some gaps between the walls in (a) and (c). The red solid and dashed lines represent the liquid-vapor and solid-liquid interface of the virtual drops. O is the origin of the coordinate system. (a) $\theta_{rear} = 51.2^\circ$, $\theta_{front} = 76.9$, $d_{SL}/a = 2.0$, $V/a^2 = 0.8$, $z_0/a = -0.63$, $z_1/a = -0.73$, $z_2/a = -1.72$; (b) $\theta_{rear} = 15.3^\circ$, $\theta_{front} = 20.0$, $d_{SL}/a = 1.0$, $V/a^2 = 0.05$, $z_1/a = -0.40$, $z_2/a = -0.90$; (c) $\theta_{rear} = 8.4^\circ$, $\theta_{front} = 84.9$, $d_{SL}/a = 4.0$, $V/a^2 = 1.8$, $z_0/a = 0$, $z_1/a = 0.33$, $z_2/a = -1.68$, $\beta_0 = 10.8^\circ$. They correspond to panels (a–c) in Fig. 4; $\alpha = 30^\circ$.

2. Hydrophobic state

When $\theta \in [90^\circ, 180^\circ]$, similar ideas could also be employed: we assume there is a gap between the two bottom walls [see Fig. 8(c)], and because of the pressure difference between the middle and the outside walls, there will be a drop formed, and its shape [enclosed using the red color in Fig. 8(d)] will be the same as the drop shown in Fig. 8(d) in the case they have the same values of θ and d. After performing similar calculations as shown in Sec. A 1, we can obtain the same equations, Eqs. (3)–(10).

3. Drop lying on an inclined surface

Last, using a similar idea, we model the wetting of drops lying on inclined surfaces, as shown in Fig. 9. We either use two walls with different contact angles [Fig. 9(b)] or use an inclined slope between the two walls with some gap in

the middle [see Figs. 9(a) and 9(c)]. The virtual 2D drops are enclosed using red curves, and the solid and dashed red curves represent the liquid-vapor and solid-liquid interfaces, respectively. The rear and front contact angles $\theta_{\rm rear}$ and $\theta_{\rm front}$ are also marked. By employing proper boundary conditions, the liquid could form shapes as given in Fig. 9. Here we have to emphasize that just for the sake of simplicity, the menisci outside of the two vertical parallel walls are given as flat surfaces (e.g., $\theta = 90^\circ$ between the outside walls and the liquid), which will not vary the physics of the menisci between the walls.

The reason for us to employ such modeling is that in this way we can easily apply the boundary conditions $z|_{x\to\infty} = 0$, $z'|_{x\to\infty} = 0$, $z''|_{x\to\infty} = 0$ to Eq. (2) to get Eq. (A1). After that, we get Eq. (A2), and this step is very useful for obtaining the other relationships. This is the key difference between our idea and the previous methods for handling this question. Otherwise, if we start modeling from a 2D sessile drop, the way to find the analytical solution is not so obvious. In the pioneering work of Frenkel [10], even though the modeling was started based on some analytical formula, later some assumptions were made and approximate solutions were given. We have to emphasize that the idea put forward in this paper should not be the unique way to solve the Young-Laplace equation for 2D sessile drops on flat and inclined surfaces, there maybe various methods, but the way we carried out is really feasible to easily find the solution.

The other related quantities such as h, d, V, and E of the drops on inclined surfaces as shown in Figs. 4 and 5 can also be obtained. For Figs. 4(a) and 4(b), we obtain

$$\frac{V}{a^2} = \frac{\sqrt{2}}{2}\left(\frac{d}{a}\right)\left(\sqrt{A-\cos\beta_1}+\sqrt{A-\cos\beta_2}\right) - (\sin\beta_1+\sin\beta_2), \tag{A5}$$

$$S_{\rm LV} = \frac{\sqrt{2}a}{2}\left(\int_0^{\beta_1}\frac{1}{\sqrt{A-\cos\xi}}\,d\xi + \int_0^{\beta_2}\frac{1}{\sqrt{A-\cos\xi}}\,d\xi\right), \tag{A6}$$

$$\frac{E_{\rm p}}{a\sigma} = (A-\cos\beta_2)\left(\frac{d}{a}\right) - \sqrt{2}\sqrt{A-\cos\beta_2}(\sin\beta_1+\sin\beta_2) - \frac{1}{6}\left(\frac{d}{a}\right)^3\tan^2\alpha + \frac{\sqrt{2}}{2}\left(\int_0^{\beta_1}\sqrt{A-\cos\xi}\cos\xi\,d\xi + \int_0^{\beta_2}\sqrt{A-\cos\xi}\cos\xi\,d\xi\right). \tag{A7}$$

For Fig. 4(c) we obtain

$$\frac{V}{a^2} = \frac{\sqrt{2}}{2}\left(\frac{d}{a}\right)\left(\sqrt{A-\cos\beta_2}-\sqrt{A-\cos\beta_1}\right) - (\sin\beta_1+\sin\beta_2), \tag{A8}$$

$$S_{\rm LV} = \frac{\sqrt{2}a}{2}\left(\int_{\beta_0}^{-\beta_1}\frac{1}{\sqrt{A-\cos\xi}}\,d\xi + \int_{\beta_0}^{\beta_2}\frac{1}{\sqrt{A-\cos\xi}}\,d\xi\right), \tag{A9}$$

$$\frac{E_{\rm p}}{a\sigma} = (A-\cos\beta_2)\left(\frac{d}{a}\right) - \sqrt{2}\sqrt{A-\cos\beta_2}(\sin\beta_1+\sin\beta_2) - \frac{1}{6}\left(\frac{d}{a}\right)^3\tan^2\alpha + \frac{\sqrt{2}}{2}\left(\int_{\beta_0}^{-\beta_1}\sqrt{A-\cos\xi}\cos\xi\,d\xi + \int_{\beta_0}^{\beta_2}\sqrt{A-\cos\xi}\cos\xi\,d\xi\right). \tag{A10}$$

A combination of either Eqs. (11) and (A5) or Eqs. (15) and (A8) leads to Eq. (19).

APPENDIX B: EXPERIMENTS

In this section, we give details of the experimental procedures to illustrate how we obtain 2D liquid strips.

To realize this aim, in the first step, we create striplike regions with different wetting properties on a silicon wafer. The fresh silicon wafer is firstly cleaned by ethanol and deionized (DI) water and dried. Then a tape with width $d = 6.3$ mm is attached on it. After that, we coat such substrate with a commercial coating agent (Glaco Mirror Coat "Zero," Soft 99) containing nanoparticles and an organic reagent [52]. Then the tape is carefully detached, and the bare silicon wafer substrate is exposed. Because the region under the tape is protected in advance, it is still hydrophilic, and the apparent contact angle is $\theta^* = 74.4 \pm 3.0^\circ$. The regions on the two sides of the

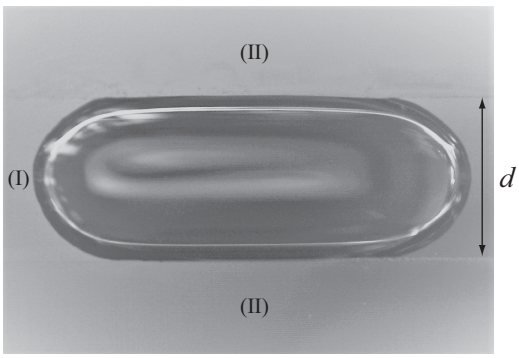

FIG. 10. Top view of the wetting state of an obtained liquid strip on a horizontal surface. The striplike region (I) with width $d = 6.3$ mm represents the hydrophilic part which is confined by two superhydrophobic regions denoted using (II).

hydrophilic region are superhydrophobic, corresponding to the apparent contact angle $\theta^* = 154.0 \pm 2.0^\circ$. By employing this way, a heterogeneous substrate with a hydrophilic region confined by two superhydrophobic regions is obtained, as shown in Fig. 10.

Next, DI water is carefully deposited onto the hydrophilic region by employing a syringe. After water attaches the hydrophilic region, the solid-liquid-vapor three-phase contact line starts to spread along the direction of the strip until it pins because of the contact angle hysteresis. However, two contact lines at the boundary of the hydrophilic and superhydrophobic regions which are perpendicular to the spreading direction always pin. Because of the pinning of the contact line at the two ends of the liquid strip, by adding different volumes of water, liquid strips with the same width d of the solid-liquid contact region but different contact angles θ (from the side view) and areas of the cross section A are achieved, as shown in Fig. 3. Typically, the length of the water strip is in the range of 18–25 mm when $\theta < 90^\circ$ and 12–15 mm when $\theta > 90^\circ$. In order to get the profile of the liquid on a slope, we just tilt the substrate, as shown in Fig. 6. Since the length of the liquid strip is much larger than its width and the contact lines constrained on the boundaries of the hydrophilic and superhydrophobic regions are quite straight, we treat the side view of the liquid strip as the profile of a 2D drop.

[1] T. Young, Philos. Trans. R. Soc. **95**, 65 (1805).
[2] P. Laplace, *Traité de mécanique céleste* (Gauthier-Villars, Paris, 1805).
[3] P.-G. de Gennes, Rev. Mod. Phys. **57**, 827 (1985).
[4] D. Bonn, J. Eggers, J. Indekeu, J. Meunier, and E. Rolley, Rev. Mod. Phys. **81**, 739 (2009).
[5] D. Lohse and X. Zhang, Rev. Mod. Phys. **87**, 981 (2015).
[6] F. Bashforth and J. C. Adams, *An Attempt to Test the Theories of Capillary Action by Comparing the Theoretical and Measured Forms of Drops of Fluid* (Cambridge University Press, 1883).
[7] C. W. Extrand and S. I. Moon, Langmuir **26**, 17090 (2010).
[8] L. D. Landau and E. M. Lifshitz, *Fluid Mechanics*, 2nd ed. (Pergamon Press, Oxford, 1987), pp. 242–243.
[9] P.-G. de Gennes, F. Brochard-Wyart, and D. Quéré, *Capillarity and Wetting Phenomena: Drops, Bubbles, Pearls and Waves* (Springer-Verlag, New York, 2004).
[10] Y. I. Frenkel, arXiv:physics/0503051.
[11] R. Finn, *Equilibrium Capillary Surfaces* (Springer, New York, 1986).
[12] A. D. Myshkis, V. G. Babskii, N. D. Kopachevskii, L. A. Slobozhanin, and A. D. Tyuptsov, *Low-Gravity Fluid Mechanics* (Springer-Verlag, Berlin, Heidelberg, 1987).
[13] E. Moy, P. Cheng, Z. Policova, S. Treppo, D. Kwok, D. R. Mack, P. M. Sherman, and A. W. Neumann, Colloids Surf. **58**, 215 (1991).
[14] H. Y. Erbil and R. A. Meric, J. Phys. Chem. B **101**, 6867 (1997).
[15] D. Y. Kwok, T. Gietzelt, K. Grundke, H.-J. Jacobasch, and A. W. Neumann, Langmuir **13**, 2880 (1997).
[16] G. Whyman and E. Bormashenko, J. Colloid Interf. Sci. **331**, 174 (2009).
[17] C. W. Extrand and S. I. Moon, Langmuir **26**, 11815 (2010).
[18] V. A. Lubarda and K. A. Talke, Langmuir **27**, 10705 (2011).
[19] S. Srinivasan, G. H. McKinley, and R. E. Cohen, Langmuir **27**, 13582 (2011).
[20] J. Park, J. Park, H. Lim, and H.-Y. Kim, Phys. Fluid **25**, 022102 (2013).
[21] D. Michael and P. Williams, Proc. R. Soc. Lond. A **351**, 117 (1976).
[22] A. Chesters, J. Fluid Mech. **81**, 609 (1977).
[23] P. Cheng and A. W. Neumann, Colloids Surf. **62**, 297 (1992).
[24] C. G. Furmidge, J. Colloid Sci. **17**, 309 (1962).
[25] D. A. Olsen, P. A. Joyner, and M. D. Olson, J. Phys. Chem. **66**, 883 (1962).
[26] C. Extrand and Y. Kumagai, J. Colloid Interface Sci. **170**, 515 (1995).
[27] P. Dimitrakopoulos and J. L. Higdon, J. Fluid Mech. **395**, 181 (1999).
[28] H.-Y. Kim, H. Lee, and B. Kang, J. Colloid Interf. Sci. **247**, 372 (2002).
[29] E. Benilov and M. Benilov, J. Fluid Mech. **773**, 75 (2015).
[30] C. Clanet and D. Quéré, J. Fluid Mech. **460**, 131 (2002).
[31] D. Siegel, Pac. J. Math. **88**, 471 (1980).
[32] H. Wong, S. Morris, and C. J. Radke, J. Colloid Interf. Sci. **148**, 317 (1992).
[33] N. D. Fowkes and M. J. Hood, Q. J. Mech. Appl. Math. **51**, 553 (1998).
[34] J. Norbury, G. C. Sander, and C. F. Scott, Q. Jl Mech. Appl. Math. **58**, 55 (2005).
[35] M. Anderson, A. Bassom, and N. Fowkes, Proc. R. Soc. London A **462**, 3645 (2006).
[36] S. Schiaffino and A. A. Sonin, J. Fluid Mech. **343**, 95 (1997).
[37] H. Gau, S. Herminghaus, P. Lenz, and R. Lipowsky, Science **283**, 46 (1999).
[38] D. Xia, L. M. Johnson, and G. P. López, Adv. Mater. **24**, 1287 (2012).
[39] E. Reyssat, J. Fluid Mech. **773**, 773R1 (2015).
[40] J. Li, X. Zhou, J. Li, L. Che, J. Yao, G. McHale, M. K. Chaudhury, and Z. Wang, Sci. Adv. **3**, eaao3530 (2017).
[41] N. Savva, S. Kalliadasis, and G. A. Pavliotis, Phys. Rev. Lett. **104**, 084501 (2010).
[42] L. A. Lubbers, J. H. Weijs, L. Botto, S. Das, B. Andreotti, and J. H. Snoeijer, J. Fluid Mech. **747**, R1 (2014).
[43] T. Liu, A. Jagota, and C.-Y. Hui, Soft Matter **11**, 3844 (2015).
[44] J. Fabre, J. Fluid Mech **797**, R4 (2016).
[45] D.-G. Lee and H.-Y. Kim, J. Fluid Mech. **624**, 23 (2009).
[46] Q.-S. Zheng, Y. Yu, and X.-Q. Feng, J. Adhes. Sci. Tech. **23**, 493 (2009).
[47] K. A. Brakke, Exp. Math. **1**, 141 (1992).
[48] T. Podgorski, J.-M. Flesselles, and L. Limat, Phys. Rev. Lett. **87**, 036102 (2001).
[49] J. H. Snoeijer, N. L. Grand-Piteira, L. Limat, H. A. Stone, and J. Eggers, Phys. Fluid **19**, 042104 (2007).
[50] I. Peters, J. H. Snoeijer, A. Daerr, and L. Limat, Phys. Rev. Lett. **103**, 114501 (2009).
[51] L. Feng, L. Z. J. Xi, Y. Zhu, N. Wang, F. Xia, and L. Jiang, Langmuir **24**, 4114 (2008).
[52] G. Dupeux, P. Bourrianne, Q. Magdelaine, C. Clanet, and D. Quéré, Sci. Rep. **4**, 5280 (2014).